264, 15293 (1989).
7. ———, *ibid.*, p. 15298.
8. P. N. Benfey and N.-H. Chua, *Science* **250**, 959 (1990).
9. The Ti plasmids used to produce transgenic plants were transferred into *A. tumefaciens* strain C58-pGV3850 [P. Zambryski *et al.*, *EMBO J.* **2**, 2143 (1983)]. Roots of *A. thaliana* race Rschew were used for transformation [D. Valvekens, M. Van Montagu, M. Van Lijsebettens, *Proc. Natl. Acad. Sci. U.S.A.* **85**, 5536 (1988)]. The progeny of transformants were self-fertilized for two generations, and we identified putative homozygous lines by scoring for lines in which all progeny contained the phosphotransferase II gene for neomycin.
10. Y. Poirier and C. Somerville, unpublished data.
11. P. J. Senior and E. A. Dawes, *Biochem. J.* **134**, 225 (1973).
12. One unit is defined as 1 μmol of acetoacetyl-CoA reduced per minute.
13. B. Janes, J. Hollar, D. Dennis, in *Novel Biodegradable Microbial Polymers*, E. A. Dawes, Ed. (Kluwer, Dordrecht, The Netherlands, 1990), pp. 175–190.
14. M. Tepfer and I. E. P. Taylor, *Science* **213**, 761 (1981); O. Baron-Epel, P. K. Gharyal, M. Schindler, *Planta* **175**, 389 (1988).
15. D. G. Lundgren, R. M. Pfister, J. M. Merrick, *J. Gen. Microbiol.* **34**, 441 (1964).
16. A. G. Ostle and J. G. Holt, *Appl. Environ. Microbiol.* **44**, 238 (1982).
17. We produced a population of plants in which approximately half accumulated PHB by sowing F3 seeds derived by the self-fertilization of the progeny of a self-fertilized F1 hybrid between transgenics RedD-3A and S8-1-2A. Leaf tissue (1 g) was homogenized in 50 mM tris-HCl (pH 8.0), 5 mM EDTA, and 1% SDS. The homogenate was cleared of large debris by low-speed centrifugation, and the insoluble material was precipitated by repeated centrifugation at 4000*g* for 15 min. The pellet was resuspended in 200 μl of 10 mM tris-HCl (pH 8.0) and 1 mM EDTA. Nile Blue A was added to a fraction of the extract (0.01% final concentration) and examined under epifluorescence microscopy. A fraction of the extract was also analyzed for the presence of PHB by GC-MS. As controls, tissues from transgenics RedD-3A and S8-1-2A were also analyzed. Red fluorescent particles could be detected only in extracts of PHB-producing tissues. Extracts that contained these particles were shown by GC-MS analysis to contain PHB. Approximately 6 μg of PHB could be recovered by this procedure from 1 g of fresh tissue.
18. R. H. Findlay and D. C. White, *Appl. Environ. Microbiol.* **45**, 71 (1983).
19. Mass spectral data were obtained at the Michigan State University–NIH Mass Spectrometry Facility.
20. Supported by grants from the U.S. Department of Energy (DE-FG02-90ER20021), the National Science Foundation (DMB9014037), and the State of Michigan Research Excellence Fund. Y.P. was supported by a fellowship of the Natural Sciences and Engineering Research Council of Canada.

20 December 1991; accepted 6 March 1992

X-ray Structure of T4 Endonuclease V: An Excision Repair Enzyme Specific for a Pyrimidine Dimer

K. Morikawa,* O. Matsumoto, M. Tsujimoto, K. Katayanagi, M. Ariyoshi, T. Doi, M. Ikehara, T. Inaoka, E. Ohtsuka

The x-ray structure of T4 endonuclease V, an enzyme responsible for the first step of a pyrimidine-dimer–specific excision-repair pathway, was determined at a 1.6-angstrom resolution. The enzyme consists of a single compact domain classified into an all-α structure. This single domain has two distinct catalytic activities: it functions as a pyrimidine dimer glycosylase and as an apurinic-apyrimidinic endonuclease. The amino-terminal segment penetrates between two major helices and prevents their direct contact. The refined structure suggests the residues involved in the substrate binding and the catalysis of the glycosylation reaction.

Ultraviolet (UV) irradiation causes formation of pyrimidine dimers within DNA that are lethal and mutagenic in vivo. The first step of the excision repair pathway of UV-damaged DNA is strand scission of the DNA in the vicinity of a pyrimidine dimer (*1*). The enzyme T4 endonuclease V, encoded by the *denV* gene of bacteriophage T4, is responsible for this step in bacteriophage-infected *Escherichia coli* (*2*, *3*). Although the enzyme is a rather small protein (138 amino acids), it has two distinct catalytic activities (*4*–*12*): it acts as a pyrimidine dimer glycosylase and as an apurinic-apyrimidinic endonuclease (Fig. 1). This latter reaction proceeds through the β-elimination of the 3′-phosphate of an abasic site rather than by the actual hydrolysis of the phosphodiester bond (*13*–*15*). Before binding to a pyrimidine dimer, the enzyme nonspecifically binds by electrostatic forces and scans the double-stranded DNA (*6*, *11*, *12*, *16*). Once the enzyme has specifically bound to a pyrimidine dimer, the DNA is incised at the 5′-glycosyl bond in the dimer, and, subsequently, scission of the phosphodiester bond occurs at the exposed backbone.

We report the three-dimensional (3-D) x-ray structure of the enzyme and discuss its functional implications. Combined with results from site-directed mutagenesis, the examination of the structural features allows the identification of residues participating in the substrate binding and the catalytic reaction.

Crystals of T4 endonuclease V (*17*) belonging to the space group $P2_1$, with unit cell parameters of a = 41.4 Å, b = 40.1 Å, c = 37.5 Å, and β = 90.01°, contain one molecule per asymmetric unit and diffract x-rays beyond 1.6 Å resolution.

An initial electron density map was calculated at 2.5 Å resolution with multiple isomorphous replacement (MIR) phases, which were obtained with five heavy-atom derivatives (Table 1). Consistent with the high value of the figure of merit, the electron densities were sufficiently well defined to allow the discernment of most residues even in a minimap, and thus an unambiguous chain tracing could be achieved. The $2F_o - F_c$ map after refinement with the restrained least-square program PROLSQ (Fig. 2) gave a final R value of 0.196 (*18*).

The enzyme T4 endonuclease V is composed of a single compact domain. The molecule has a roughly ellipsoidal shape with dimensions 50 by 42 by 40 Å. The enzyme consists of three α helices, five reverse turns, and extended chain segments and loops, but it contains no β structure (*19*) (Fig. 3). The enzyme should thus be classified into the all-α type of structure (*20*); 45% of its residues are located in α helices (Fig. 4). The first α helix (H1, residues 14 through 38) is centrally kinked at Pro^{25}, creating an inclination of 20°. All of the five reverse turns lie on the external surface of the molecule and in close proximity to NH_2- or COOH-terminal ends of the α helices, except for one reverse turn (Q98 to F100) (*21*).

The arrangement of α helices in this enzyme is unusual. The three helices, H1 (14 through 38), H2 (64 through 82), and H3 (108 through 124), stand side-by-side (Fig. 3), and their termini are covered by a caplike loop around the COOH-terminus.

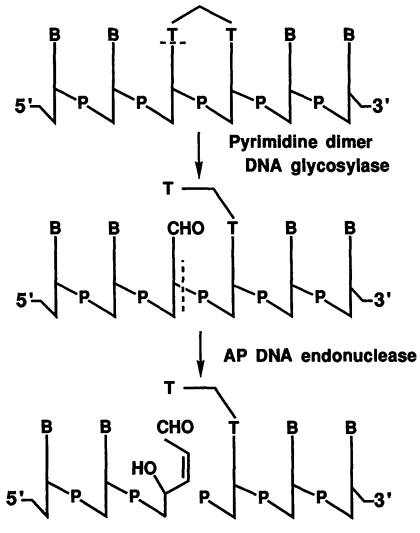

Fig. 1. Two distinct catalytic activities of T4 endonuclease V. AP, apurinic or apyrimidinic.

K. Morikawa, O. Matsumoto, M. Tsujimoto, K. Katayanagi, M. Ariyoshi, T. Doi, M. Ikehara, Protein Engineering Research Institute, 6-2-3 Furuedai, Suita, Osaka 565, Japan.
T. Inaoka and E. Ohtsuka, Faculty of Pharmaceutical Sciences, Hokkaido University, Sapporo, Hokkaido 060, Japan.

*To whom correspondence should be addressed.

The three long helices, H1, H2, and H3, appear to stand on this rigid loop, forming a layer of helices. This loop near the COOH-terminus has the sequence WYKYY (128 through 132) and comprises aromatic and basic residues. Many polar interactions are formed, mainly between the backbone of the loop and the two α-helical ends, H1 and H3; the Trp and the Tyr side chains in the loop face the solvent. The main chain imino and carbonyl groups of Lys^{130} are also tightly bound to the Gln^{15} side chain and the peptide imino group of Asp^{14}, both of which lie at the amino end of H1, although the side chain of Lys^{130} points into the solvent. Helix H2 has a polar interaction with the loop through a water molecule that coordinates the carboxyl group of Glu^{77} with the phenol ring of Tyr^{132}. Helix H2 is closely packed with helix H1 in an almost antiparallel direction by a multitude of electrostatic and hydrophobic interactions. Mutations at Asp^{14}, Lys^{80}, and Arg^{81}, which help to connect the loop and the helices, severely reduce expression (*22*).

Seven residues at the NH_2-terminus, TRINLTL, penetrate between helices H1 and H3 (Fig. 3) and prevent their direct contacts. Two polar residues at the NH_2-terminus, Thr-Arg, lie on the molecular surface. This folding scheme is inexplicable with the close-packing category for the assembly of α helices.

The NH_2-terminal segment forms several hydrogen bonds with the side chains of these two helices. All of the hydrogen bonds use backbone atoms as donors and acceptors, such as the NH of Arg^3 with the carboxyl side chain of Glu^{23}, the CO of Arg^3 with a water molecule (140WAT), the NH of Ile^4 with the imidazole group of His^{56}, the NH of Asn^5 with the carboxyl group of Glu^{20}, the CO of Asn^5 with the guanidino side chain of Arg^{70}, and the NH of Leu^6 with the hydroxyl group of Ser^{114}. These striking polar interactions imply that the internal main chain peptide groups in a protein structure cannot be exposed without having polar interactions with the surrounding atoms.

A molecular graphics display of the electrostatic potentials on a solvent-accessible surface (*23*) is useful for identifying regions that interact with polynucleotides because basic residues can bind polynucleotides through electrostatic forces. These positive charges, which are contributed by Lys^{33}, Lys^{39}, Lys^{86}, Lys^{121}, Arg^3, Arg^{22}, Arg^{26}, Arg^{32}, and Arg^{117}, lie on the internal curvature of the comma-shaped molecule.

A single acidic residue, Glu^{23}, is surrounded by many basic residues, such as Arg^3, Arg^{22}, Arg^{26}, Arg^{117}, and Lys^{121}, as though a single negative charge floats in a sea of positive charges (Fig. 5). This region forms a groove-like depression with dimensions just large enough to accommodate a single strand of B-form DNA. This depression passes across the molecular surface near the two helical ends of H1 and H3. In this substrate-free structure, Glu^{108} of a neighboring molecule approaches this empty depression and has intermolecular ionic interactions with the side chains of Arg^3 and His^{16}.

The side chain of Glu^{23} forms a hydrogen bond with the backbone imino group of Arg^3 and also interacts with the backbone carbonyl of Arg^3 through a tightly bound water molecule (140WAT). The second water (161WAT) is bound to the guanidino group of Arg^3, the side chain carbonyl of Asn^5, and the main chain carbonyl of His^{16}. These two water molecules are trapped at the bottom of a cavity in close proximity to Arg^3 and Glu^{23}

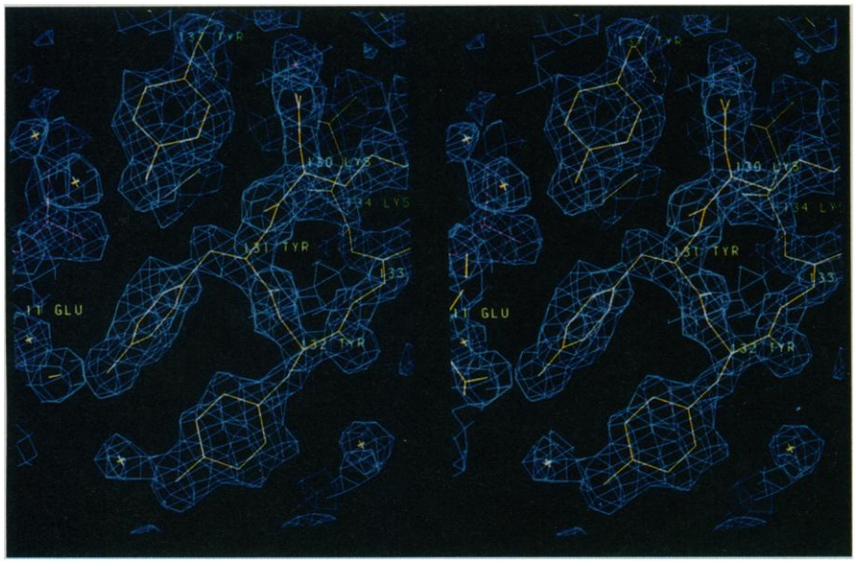

Fig. 2. Stereo drawing of electron density contoured at 1.0σ. The refined model at 1.6 Å resolution is superimposed on the $2F_o - F_c$ map after refinement by PROLSQ. This molecular portion corresponds to the COOH-terminal loop comprising the WYKYY sequence.

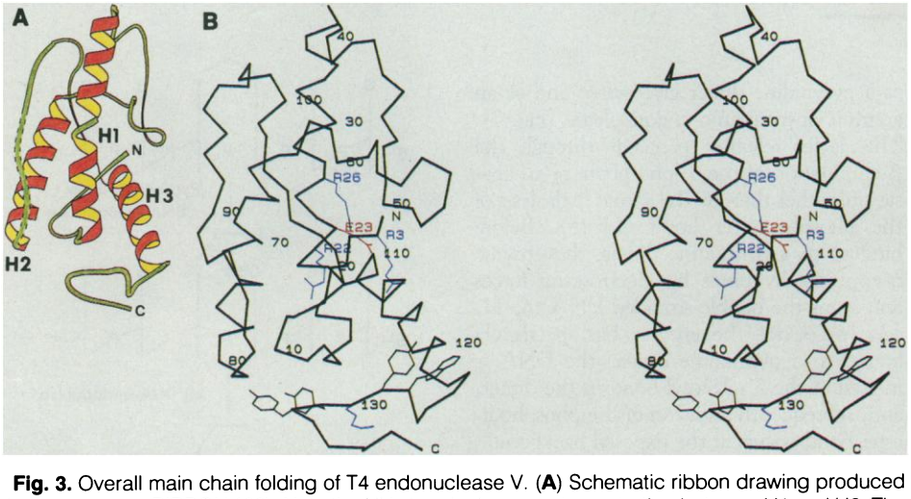

Fig. 3. Overall main chain folding of T4 endonuclease V. (**A**) Schematic ribbon drawing produced by the program RIBBON (*28*). Note the NH_2-terminal segment penetrating between H1 and H3. The broken region indicates the mobile segment with the unusually high temperature factors. (**B**) Stereodrawing of the Cα backbone in a similar orientation. Side chains are drawn in different colors (acidic, red; basic, blue) for the four residues involved in glycosylase activity or substrate binding. The side chains of the WYKYY sequence are also indicated.

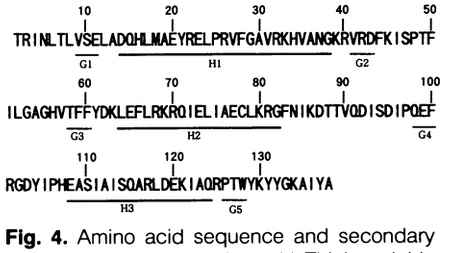

Fig. 4. Amino acid sequence and secondary structure of T4 endonuclease V. Thick and thin underlines indicate the ranges of α helices (H1 through H3) and reverse turns (G1 through G5), respectively.

(Fig. 5). Another water molecule (238WAT) has polar interactions with the carboxyl group of Glu^{23}. Mutation of Glu^{23} to Gln (E23Q) displaces this water molecule in the refined crystal structure.

The mutations E23Q and E23D caused almost complete loss of the glycosylase activity (*22*). The mutation R3Q also eliminated the activity. The same substitutions for Arg^{26} and Arg^{22} decreased the activities to less than 1 and 6%, respectively, whereas the substitution of Lys for Arg^{22} still retained about 50% activity. These residues are localized in the three-dimensional structure (Fig. 3B).

The three mutants, E23Q, E23D, and R3Q, were crystallized as the isomorphous crystal form with that of the wild type. We have refined the two crystal structures of E23Q and R3Q at 1.8 and 2.2 Å resolutions and *R* values of 0.221 and 0.190, respectively. Both fragment-deleted difference Fourier maps (omit maps) showed that structural differences between the mutants and the wild type are confined to only a small region near the replaced side chains. Even for the E23Q mutant, which yielded a larger change in the two maps, the displacements of protein atoms are at most 0.7 Å. Difference circular dichroism spectra measured for the E23Q and R3Q mutants mixed with a synthetic DNA duplex containing a pyrimidine dimer (*22*) revealed that E23Q almost completely retains the ability to bind the substrate, whereas the R3Q mutation greatly decreases this binding ability. The loss of the glycosylase activity in the E23Q mutant is likely attributable only to the disappearance of the negative charge at Glu^{23} in the wild-type enzyme and the concomitant changes in the ionic interactions with the surrounding water molecules. The decreased substrate-binding ability of R3Q highlights the importance of the positively charged guanidino group of Arg^3 for substrate binding. The participation of Arg^3 in nontarget binding to DNA was revealed by Dowd and Lloyd (*24*).

Site-directed mutagenesis experiments of the enzyme by two research groups suggested that the WYKYY sequence may participate in pyrimidine-dimer–specific binding and possibly in nicking activity as well (*25*). This sequence forms a rigid loop near Glu^{23} (Fig. 5). Most of the side chain atoms of this aromatic segment can still

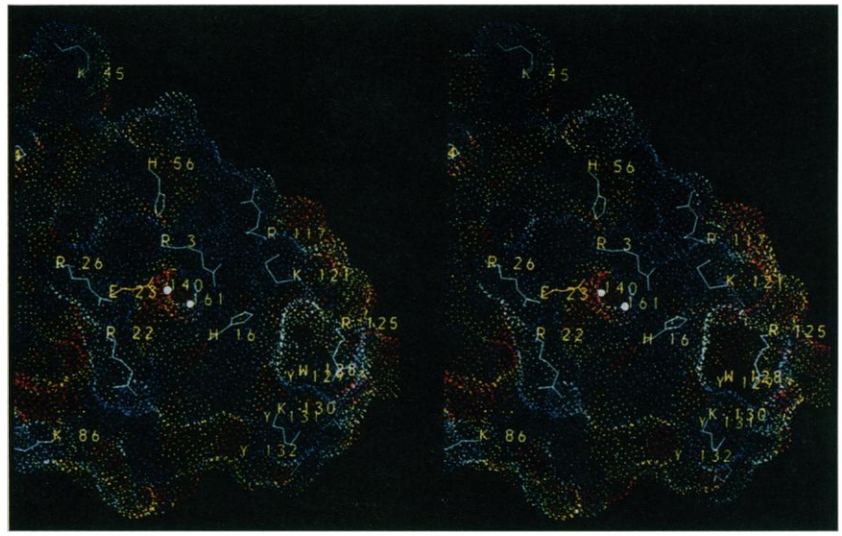

Fig. 5. Distribution of the electrostatic potential on the solvent-accessible surface of T4 endonuclease V. Red denotes electrostatic potential values below −0.1 V, and blue denotes values above +0.1 V; intermediate values follow the spectrum from blue to red. The stereopair represents the environment around Glu^{23} (orange bonds) and the surrounding basic residues (blue bonds), such as Arg^3, Arg^{22}, and Arg^{26}. A groove-like depression passes in contact with the putative catalytic center (Glu^{23}), and a part of the WYKYY segment is located on the opposite ridge. The residues His^{16} and Arg^3 lie near the bottom of the depression. Two water molecules (140WAT and 161WAT), which are tightly bound to Glu^{23}, Arg^3, and His^{16}, are indicated by white dots.

Table 1. Structure determination statistics. Intensity data to 1.6 Å resolution have been collected from native crystals with a four-circle diffractometer (Enraf Nonius CAD4) on a generator with a sealed fine-focus Cu tube. The complete data set to 1.6 Å from the native crystal contains 13,869 reflections, corresponding to 83% of the theoretical number of reflections. Heavy-atom derivatives were prepared by soaking crystals in crystallizing solutions containing 25% (w/v) polyethylene glycol and the respective heavy-atom compounds. All five derivatives yielded difference Patterson maps with low noise, and the major sites of heavy atoms were easily found. Heavy-atom parameters were determined from five derivatives with the phase refinement program PROTEIN (*26*) for the MIR, which takes the anomalous dispersion effect into account. Phase statistics gave an average figure of merit of 0.81. The initial model was fitted into the MIR map at a 2.5 Å resolution on a graphics system (Evans and Sutherland PS390) by the use of the program FRODO (*27*). The structure was refined with the Hendrickson-Konnert restrained least-square refinement program (*18*) running on a FACOM VP 400E supercomputer. The *R* value is 0.196 for 13,163 reflections from 5.0 to 1.6 Å after a restrained *B*-factor refinement with 100 water molecules included. The root mean square (rms) deviations from ideal bond lengths and 1-3 bond angle distances are 0.018 and 0.037 Å, respectively. The quantity $R_{Cullis} = \Sigma||F_{PH} \pm F_P| - F_{H(calc)}|/\Sigma|F_{PH} - F_P|$ for centric reflections, where F_{PH} is the structure amplitude of a derivative, F_P is the structure amplitude of the native crystal, and F_H is the structure amplitude of a heavy atom. Phasing power is the ratio of the amplitude of the rms heavy-atom scattering factor to the rms lack-of-closure error.

Data set	Resolution (Å)	Independent reflections (no.)	Crystals (no.)	R_{merge}	Average isomorphous difference	Heavy-atom sites (no.)	Phasing power	R_{Cullis}
			Multiple isomorphous replacement					
Native	2.5	4,178	1	*				
$KAuCN_2$	2.5	4,091	3	0.0808	0.234	6	2.56	0.45
cis-$Pt(NH_3)_2Cl_2$	2.7	3,258†	2	0.0421	0.334	2	1.50	0.69
trans-$Pt(NH_3)_2Cl_2$	3.0	2,381	2	0.0484	0.270	5	2.53	0.52
K_3IrCl_6	2.5	4,106	3	0.0648	0.093	4	0.78	0.89
Methyl mercuric acetate	2.5	3,938†	6	0.0571	0.224	3	3.44	0.39
			Crystallographic refinement					
Native	1.6	13,869	2	0.0429				

*No evaluation of R_{merge} because of data collection from one single crystal. †The number of intensity data including Bijvoet pairs.

interact with DNA, although the main-chain atoms are occupied in the polar interactions between the loop and the two helical ends.

REFERENCES AND NOTES

1. P. C. Hanawalt, P. K. Cooper, A. K. Ganesan, C. A. Smith, *Annu. Rev. Biochem.* **48**, 783 (1979).
2. S. Yasuda and M. Sekiguchi, *Proc. Natl. Acad. Sci. U.S.A.* **67**, 1839 (1970).
3. E. C. Friedberg and J. J. King, *J. Bacteriol.* **106**, 500 (1971).
4. L. K. Gordon and W. A. Haseltine, *J. Biol. Chem.* **255**, 12047 (1980).
5. P. C. Seawell *et al.*, *J. Virol.* **35**, 790 (1980).
6. E. H. Radany and E. C. Friedberg, *Nature* **286**, 182 (1980).
7. S. McMillan *et al.*, *J. Virol.* **40**, 211 (1981).
8. Y. Nakabeppu and M. Sekiguchi, *Proc. Natl. Acad. Sci. U.S.A.* **78**, 2742 (1981).
9. H. R. Warner, L. M. Christensen, M.-L. Persson, *J. Virol.* **40**, 204 (1981).
10. Y. Nakabeppu, K. Yamashita, M. Sekiguchi, *J. Biol. Chem.* **257**, 2556 (1982).
11. E. A. Gruskin and R. S. Lloyd, *ibid.* **261**, 9607 (1986).
12. M. L. Dodson and R. S. Lloyd, *Mutation Res.* **218**, 49 (1989).
13. J. Kim and S. Linn, *Nucleic Acids Res.* **16**, 1135 (1988).
14. M. Monoharan, A. Mazamder, S. C. Ransom, J. A. Gerlt, P. H. Bolton, *J. Am. Chem. Soc.* **110**, 2690 (1988).
15. A. Mazumder *et al.*, *ibid.* **111**, 8029 (1989).
16. A. K. Ganesan, P. C. Seawell, R. J. Lewis, P. C. Hanawalt, *Biochemistry* **25**, 5751 (1986).
17. K. Morikawa, M. Tsujimoto, M. Ikehara, T. Inaoka, E. Ohtsuka, *J. Mol. Biol.* **202**, 683 (1988).
18. W. A. Hendrickson and J. H. Konnert, in *Computing in Crystallography*, R. Diamond, S. Ramaseshan, K. Venkatesan, Eds. (National Academy of Science of India, Bangolore, 1980), pp. 13.01–13.23.
19. W. Kabsch and C. Sander, *Biopolymers* **22**, 2577 (1983).
20. M. Levitt and C. Chochia, *Nature* **261**, 552 (1976).
21. Abbreviations for the amino acid residues are as follows: A, Ala; C, Cys; D, Asp; E, Glu; F, Phe; G, Gly; H, His; I, Ile; K, Lys; L, Leu; M, Met; N, Asn; P, Pro; Q, Gln; R, Arg; S, Ser; T, Thr; V, Val; W, Trp; and Y, Tyr.
22. T. Doi *et al.*, unpublished results.
23. H. Nakamura and S. Nishida, *J. Phys. Soc. Jpn.* **56**, 1609 (1987).
24. D. R. Dowd and R. S. Lloyd, *Biochemistry* **28**, 8699 (1989); *J. Mol. Biol.* **208**, 701 (1989).
25. A. Recinos III and R. S. Lloyd, *Biochemistry* **27**, 1832 (1988); D. G. Stump and R. S. Lloyd, *ibid.*, p. 1839; R. S. Lloyd and M. L. Augustine, *Proteins* **6**, 128 (1989); M. Ishida, Y. Kanamori, N. Hori, T. Inaoka, E. Ohtsuka, *Biochemistry* **29**, 3817 (1990).
26. W. Steigemann, thesis, Technische Universität, München (1974).
27. T. A. Jones, *J. Appl. Crystallogr.* **11**, 268 (1978).
28. J. P. Priestle, *ibid.* **21**, 572 (1988).

29. We are indebted to H. Nakamura for his help in molecular graphics work and A. Recktenwald for his collaboration in site-directed mutagenesis. Y. Ohta, T. Tanaka, S. Kimura, and H. Sakashita are acknowledged for their purification of T4 endonuclease V and M. Matsushima for his refinement of heavy-atom parameters. We also thank A. Klug, P. Evans, C. Chochia, J. Finch, and A. Pähler for their critical reading of the manuscript and helpful comments. Coordinates for the refined model of T4 endonuclease V have been submitted to the Protein Data Bank. This research was partly supported by a Human Frontier Science Program research grant for international collaboration groups.

8 November 1991; accepted 28 February 1992

Tertiary Structure Around the Guanosine-Binding Site of the *Tetrahymena* Ribozyme

Jin-Feng Wang and Thomas R. Cech*

A cleavage reagent directed to the active site of the *Tetrahymena* catalytic RNA was synthesized by derivatization of the guanosine substrate with a metal chelator. When complexed with iron(II), this reagent cleaved the RNA in five regions. Cleavage at adenosine 207, which is far from the guanosine-binding site in the primary and secondary structure, provides a constraint for the higher order folding of the RNA. This cleavage site constitutes physical evidence for a key feature of the Michel-Westhof model. Targeting a reactive entity to a specific site should be generally useful for determining proximity within folded RNA molecules or ribonucleoprotein complexes.

Many RNA molecules require specifically folded structures for their biological activity. RNA base-pairing interactions (secondary structure) can be established by sequence analysis of functionally equivalent RNAs from phylogenetically diverse organisms (*1*). In contrast, our understanding of the three-dimensional (3-D) structure of RNAs is limited. Only for some small RNAs have atomic-resolution structures been determined by x-ray crystallography or nuclear magnetic resonance spectrometry (*2*). Methods such as site-specific mutagenesis, chemical and enzymatic probing, and comparative sequence analysis have proven to be informative in studying other RNA 3-D structures. Ribozymes, or catalytic RNAs, are attractive for studies of RNA folding because their structure is directly reflected in their activity.

The L-21 Sca I ribozyme is derived from the group I intervening sequence of *Tetrahymena thermophila* pre–ribosomal RNA (*3*). This ribozyme cleaves other RNA molecules using as a nucleophile the 3′ hydroxyl of G (guanosine or one of its 5′-phosphorylated forms) [Fig. 1A; (*4*)]. The G264-C311 base pair (the G-site) binds the G substrate (*5*, *6*).

Howard Hughes Medical Institute, Department of Chemistry and Biochemistry, University of Colorado, Boulder, CO 80309–0215.

*To whom correspondence should be addressed.

We used affinity cleavage (cleavage by a bound reagent) to identify regions of the RNA in proximity to the G-site. The redox active metal iron(II) [Fe(II)], when chelated by EDTA or DTPA (diethylenetriaminepentaacetic acid) and incubated with a reducing reagent such as ascorbate in the presence of O_2 (or H_2O_2), generates short-lived free radicals that initiate oxidative degradation of any neighboring nucleic acid sugars (*7*). Cleavage is largely independent of base identity or secondary structure (*8*). Tethering EDTA-Fe(II) or DTPA-Fe(II) to guanosine 5′-phosphate (GMP) was expected to target the destructive reagent to the G-site, thereby providing information about the 3-D structure of the catalytic core of the ribozyme.

The metal chelator DTPA was tethered to the 5′ phosphate of GMP [G-DTPA, Fig. 1B; (*9*)], and its reactivity as a ribozyme substrate was compared to that of GMP. The G-DTPA reagent was active as a nucleophile and yielded the same product from 5′ end-labeled RNA substrate (Fig. 1A) as did GMP and guanosine (*10*).

When a mixture of G-DTPA and GMP was reacted with an internally labeled RNA substrate, both DTPA-Gp*AGU and Gp*AGU were formed at a ratio that represented the relative reactivity of the two G substrates (Fig. 2). The activity of G-DTPA was about one-tenth that of GMP. Quantitative kinetic measurements

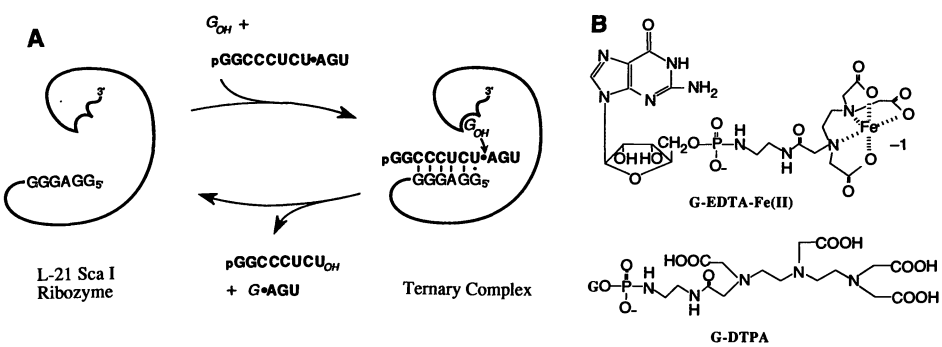

Fig. 1. (**A**) Endonuclease reaction catalyzed by the ribozyme. (**B**) Structures of GMP-EDTA-Fe(II) [G-EDTA-Fe(II)] and GMP-diethylenetriaminepentaacetic acid (G-DTPA).